A Method to Estimate the Atomic Number and Mass Thickness of Intervening Materials in Uranium and Plutonium Gamma-Ray Spectroscopy Measurements

Michael Streicher, Steven Brown, Yuefeng Zhu, David Goodman, and Zhong He, *Senior Member, IEEE*

Abstract—To accurately characterize shielded special nuclear materials (SNM) using passive gamma-ray spectroscopy measurement techniques, the effective atomic number and the thickness of shielding materials must be measured. Intervening materials between the source and detector may affect the estimated source isotopics (uranium enrichment and plutonium grade) for techniques which rely on raw count rates or photopeak ratios of gamma-ray lines separated in energy. Furthermore, knowledge of the surrounding materials can provide insight regarding the configuration of a device containing SNM. The described method was developed using spectra recorded using high energy resolution CdZnTe detectors, but can be expanded to any gamma-ray spectrometers with energy resolution of better than 1% FWHM at 662 keV. The effective atomic number, Z, and mass thickness of the intervening shielding material are identified by comparing the relative attenuation of different gamma-ray lines and estimating the proportion of Compton scattering interactions to photoelectric absorptions within the shield. While characteristic K_α x-rays can be used to identify shielding materials made of high Z elements, this method can be applied to all shielding materials. This algorithm has adequately estimated the effective atomic number for shields made of iron, aluminum, and polyethylene surrounding uranium samples using experimental data. The mass thicknesses of shielding materials have been estimated with a standard error of less than 1.3 g/cm^2 for iron shields up to 2.5 cm thick. The effective atomic number was accurately estimated to 26 ± 5 for all iron thicknesses.

Index Terms—CdZnTe detectors, gamma-ray imaging, gamma-ray spectroscopy, special nuclear materials monitoring.

I. INTRODUCTION

SHIELDED special nuclear material (SNM) in the form of highly enriched uranium or weapon-grade plutonium can be extremely difficult to detect, identify, and characterize [1]. This work assumes that shielded SNM has been detected and identified; now the material needs to be characterized.

The characterization includes estimating the isotopics of the source and imaging its physical configuration. In order to properly estimate the sample isotopics using raw count rates or photopeak ratios of gamma-ray lines separated in energy, the true source emission rate needs to be determined [2], [3]. Therefore, one must correct for shielding material attenuation in order to accurately estimate the enrichment of the sample [4], [5]. In addition to correcting the recorded gamma-ray spectrum to obtain the true emission spectrum from the source, identifying the shielding materials can inform the response to a discovered source and provide insight to the configuration of the SNM containing device if it cannot be directly observed.

Many efforts to calculate the composition of shielding materials rely on template matching techniques [6]. These methods require a number of simulated or measured spectra which are fit to new data in order to estimate activity or characterize intervening materials. Other solutions involve using cross sections and user input parameters to estimate the detector response to different sources and intervening materials [7]. The residual between the expected spectrum and the recorded data is used to select the most likely source configuration. Others have suggested using Bayesian approaches for estimating source configuration [8], but Ref. [8] assumed that intervening materials were known and attempted to calculate the plutonium mass instead. These approaches are required for low resolution spectrometers. This work uses direct spectroscopic information which is possible when a high resolution spectrometer is employed.

II. MEASUREMENTS AND DETECTION SYSTEM

The data used to develop this method were recorded at the Y-12 National Security Complex and the Device Assembly Facility (DAF) at the Nevada National Security Site using a prototype digital CZT array system. The system consisted of four $2 \times 2 \times 1.5$ cm^3 three-dimensional position-sensitive CdZnTe gamma-ray detectors. Each detector was read out by a VAD_UMv1.2 ASIC developed jointly by Integrated Detector Electronics AS (IDEAS) (Oslo, Norway) and the University of Michigan [9]. The system demonstrated an energy resolution of 0.47% FWHM at 662 keV for single pixel events and 0.63% FWHM at 662 keV for all events [10].

At the Y-12 National Security Complex, various configurations and enrichments of uranium were measured [11]. Steel,

polyethylene, and aluminum sheets were used to shield the uranium source. At the DAF, plutonium and uranium samples were measured. The sources were spherical in shape, and shells of shielding materials were available to modulate source photons.

III. Ratio of Gamma-ray Line Attenuation in Shielded Uranium Samples

Because uranium samples have multiple gamma-ray lines, it is possible to estimate attributes of shielding materials based on the attenuation of different gamma-ray energies [12]. The most prominent gamma-ray lines from ^{235}U occur at 143.76 keV, 166.36 keV, 185.71 keV, and 205.32 keV [13]. Note that the 202.1 keV line is often grouped with the 205 keV line to calculate peak ratios if the energy resolution of the detector is not sufficient to resolve it. Shielding corrections are required to account for attenuation through the shielding material when conducting enrichment measurements or other measurements where accurate emission rates or emission ratios from the uranium source itself are required. In some situations, the materials surrounding uranium need to be identified in order to determine if the configuration is an immediate threat. In order to identify the shielding material and its thickness, a peak ratio method was used. Consider the attenuation of two different gamma-ray lines through a shielding material. The intensity of the lines after passing through the shielding can be calculated using Eq. 1 and Eq. 2 [14].

$$I_1 = I_{01} e^{-\left(\frac{\mu}{\rho}\right)_1 \cdot \rho x} \tag{1}$$

$$I_2 = I_{02} e^{-\left(\frac{\mu}{\rho}\right)_2 \cdot \rho x} \tag{2}$$

In Eq. 1 and Eq. 2, I is the intensity of the line after passing through the shielding material, I_0 is the initial intensity of the line at the surface of the source, μ is the linear attenuation coefficient of the shielding material which depends on the incident gamma-ray energy, ρ is the mass density of the shielding material, and x is the thickness of the shield. The subscripts indicate gamma-ray lines of different energies. Eq. 1 and Eq. 2 can be combined as shown in Eq. 3.

$$\frac{I_1}{I_2} = \frac{I_{01}}{I_{02}} e^{-\left[\left(\frac{\mu}{\rho}\right)_1 - \left(\frac{\mu}{\rho}\right)_2\right] \cdot \rho x} \tag{3}$$

Take the natural logarithm to linearize the expression as shown in Eq. 4 [15], [16].

$$\ln\left(\frac{I_1}{I_2}\right) - \ln\left(\frac{I_{01}}{I_{02}}\right) = \left[\left(\frac{\mu}{\rho}\right)_2 - \left(\frac{\mu}{\rho}\right)_1\right] \cdot \rho x \tag{4}$$

Note that the mass attenuation coefficient (μ/ρ) for a given gamma-ray energy is simply a function of the effective atomic number of the shielding material, Z_{eff}.

Given the mass attenuation coefficient as a function of atomic number for a given gamma-ray line from a detected isotope, one can use multiple lines to estimate the atomic number of the shield and the density-thickness product. One can measure intensity ratios of gamma-ray lines and then iterate through Z numbers and density-thickness products to calculate the most probable shielding material and mass-thickness combinations based on the agreement between the
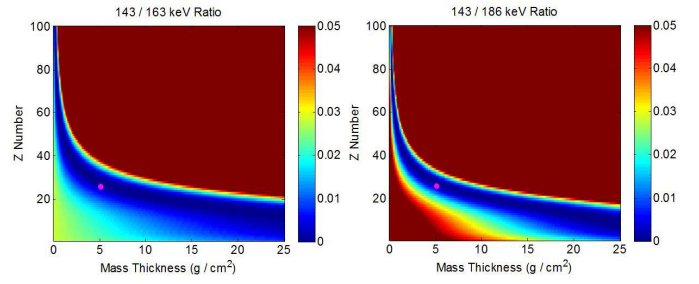

Fig. 1. Simultaneous estimate of the effective atomic number and the thickness of the shielding material using the gamma-ray line attenuation ratio method. The magenta dot shows the true effective atomic number and mass-thickness of the shield.
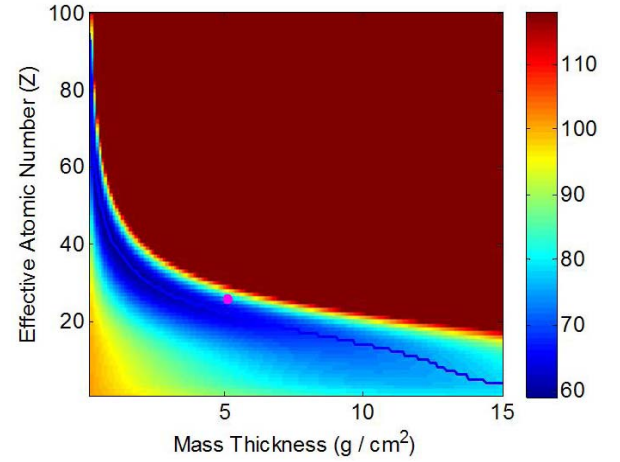

Fig. 2. Combined residuals from all of the line intensity comparisons to determine the best estimate for the effective atomic number and the thickness of the shield. The true combination is shown with the magenta dot. A line representing the lowest residual effective atomic number as a function of mass-thickness is overlaid in blue. There is a small systematic error using this method which is further explored in Section VI.

measured change in peak ratio (left-hand side of Eq. 4) and the theoretical attenuation for a particular shielding combination (right-hand side of Eq. 4). The residual (squared difference) between the left-hand side and right-hand side of Eq. 4 is used to quantify the agreement between measurement and theory for a particular combination. For some iteration of mass-thickness, $(\rho x)_i$ and effective atomic number, $Z_{eff,j}$ which provides mass attenuation coefficients, $(\mu/\rho)_{2j}$ and $(\mu/\rho)_{1j}$, the residual value for this iteration, r_{ij}, is calculated in Eq. 5.

$$r_{ij}^2 = \left[\ln\left(\frac{I_1}{I_2}\right) - \ln\left(\frac{I_{01}}{I_{02}}\right) - \left[\left(\frac{\mu}{\rho}\right)_{2j} - \left(\frac{\mu}{\rho}\right)_{1j}\right] \cdot (\rho x)_i\right]^2 \tag{5}$$

In Eq. 5, (I_1/I_2) is the measured net photopeak count ratio for two characteristic gamma-ray lines and (I_{01}/I_{02}) is the expected photopeak count ratio if no shielding is present. The residual results for two line ratios from a uranium measurement are shown in Fig. 1. The dark blue areas in Fig. 1 have the lowest residuals and are the most probable combinations of shielding material parameters to produce the observed attenuation. In Fig. 2, the residuals from all six line ratios are combined into one metric by weighting the residuals by
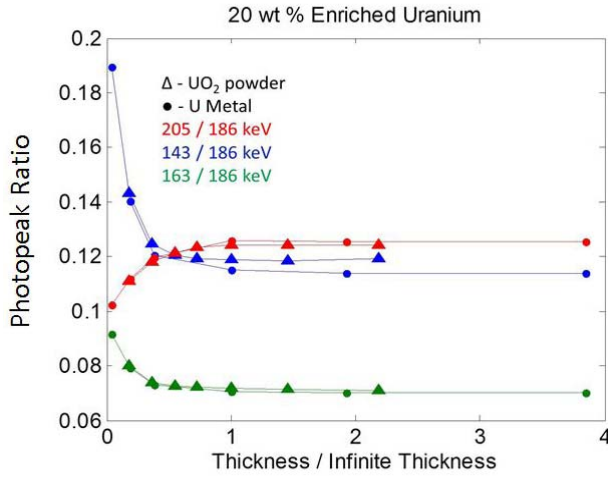
Fig. 3. Intensity ratios for gamma-ray lines as a function of the sample thickness for uranium metal (circles) and UO_2 powder (triangles). The infinite thickness is given in the PANDA manual for various uranium compositions.

the propagated error as shown in Eq. 6. There is no definitive spot where the residual is lowest.

$$R_{ij}^2 = \sum_{k=1}^{6} (r_{ijk}^2 / \sigma_k^2) \qquad (6)$$

In Eq. 6, r_{ijk} is the residual of the kth gamma-ray line combination for one iteration of effective atomic number and mass thickness and σ_k is the propagated uncertainty in the measured net photopeak count ratio of the kth gamma-ray line combination.

For this method to work, the isotope must be identifiable. This means that the lines must be visible above the continuum in order to measure the intensity of the line. In this work, this requires that the intensity of the 185.7 keV line from ^{235}U must be greater than the background level. The term (I_{01}/I_{02}) will be known for a given isotope and source thickness. This term will also account for the branching ratios of the different gamma-ray lines from ^{235}U. For uranium samples, the initial intensity ratio does not vary with enrichment. It does vary slightly with the material composition and thickness of the uranium. Fig. 3 shows how the line ratios are affected by the thickness of the sample. The data for Fig. 3 were generated using the Geant4 simulation package [17].

The combined residual shown in Fig. 2 can be simplified by taking the Z number with the smallest residual for each mass thickness which accounts for the observed line attenuation. The results for three different measured steel thicknesses are given in Fig. 4. The source was a 20 wt% ^{235}U metal disk, 3 cm in diameter and 0.3 cm thick. The steel shields were large planar slabs. The lines in Fig. 4 show the possible combinations of shield thickness and material which could account for the measured differences in the attenuation of the various gamma-ray lines. For shields made from large atomic number materials, characteristic x-rays could be used to identify the shielding type. This has been experimentally demonstrated with tungsten and lead shields [16].

While useful information can be extracted using the attenuation method, it cannot definitively predict the shielding
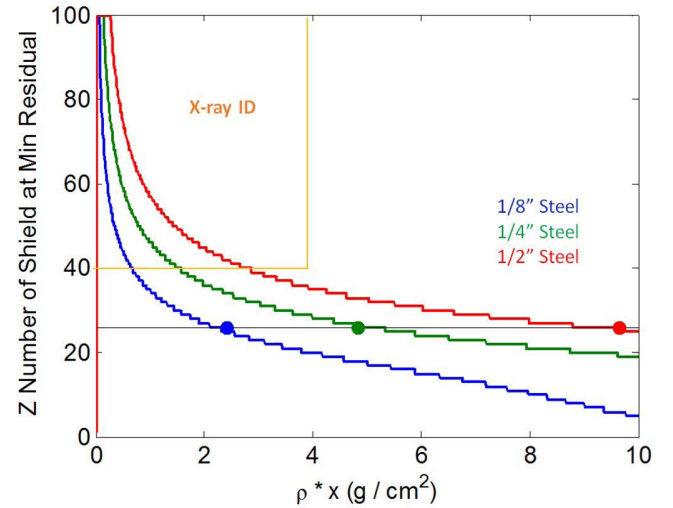

Fig. 4. Lowest residual atomic number for each mass thickness for three different steel shielding thicknesses. The true combinations of material and mass thickness are shown using the large dots. The yellow region is the area where characteristic x-rays would be available to reveal the identity of the shielding material.
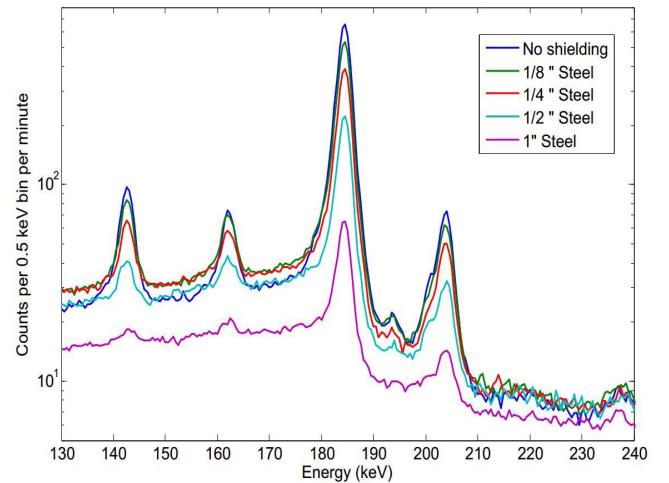

Fig. 5. Gamma-ray energy spectra of a 20 wt % ^{235}U uranium metal sample from Y-12 with various thicknesses of steel shielding between the source and detection system.

thickness and effective atomic number of the shield. As a result the estimated unattenuated intensities of gamma-ray lines from different isotopes cannot be uniquely determined. Therefore, another method is required.

IV. FORWARD COMPTON SCATTERING

While the photoelectric absorption cross section depends considerably on the effective atomic number of the shield, the probability of Compton scattering depends on the number of electrons a photon encounters as it travels through the shield, which scales linearly with atomic number and mass thickness. Differences in the spectrum from Compton scattering in the shield are shown in Fig. 5. The spectra were taken with a 20 wt% ^{235}U sample of uranium metal through various thicknesses of shielding. Note that above 210 keV, the background

gamma intensity is about the same for all of the measurements except for when one inch of steel shielding is used. Notice that the intensity of the 186 keV photopeak is reduced when an eighth of an inch of steel is used to shield the source. However, the continuum to the left of the peak (166 - 176 keV) is higher when the shield is present due to forward Compton scattered 186 keV gamma rays in the intervening material.

The probability that a photon incident on a shield scatters once in dx about x into solid angle $d\Omega$ about Ω and escapes is the product of four probabilities. First is the probability that a photon reaches some shield depth, x, without undergoing an interaction, given by Eq. 7.

$$P(unnattenuated\ to\ x) = e^{-\mu_{t,1}x} \qquad (7)$$

In Eq. 7, $\mu_{t,1}$ is the total linear attenuation coefficient for the shield. Then, the photon must interact within some dx within the shield, the probability of which is given by Eq. 8.

$$P(interact\ in\ dx) = \mu_{t,1}dx \qquad (8)$$

Then, the interaction must result in the photon scattering into some $d\Omega$ solid angle which is given by Eq. 9.

$$P(scatter\ within\ d\Omega) = \frac{1}{\sigma_t}\frac{d\sigma_c}{d\Omega}d\Omega \qquad (9)$$

In Eq. 9, σ_t is the total interaction cross section and $\frac{d\sigma_c}{d\Omega}$ is the Klein-Nishina cross section. Finally, the scattered photon has to escape the remainder of the shield without undergoing another interaction, the probability of which is given in Eq. 10

$$P(scattered\ photon\ escapes\ shield) = e^{-\mu_{t,2}(D-x)} \qquad (10)$$

where D is the thickness of the shield, and $\mu_{t,2}$ is the linear attenuation coefficient for the scattered photon. In truth, the path length will be longer, but by making Ω small, one can make the assumption that l, the true path length, approximately equals $D - x$ as $d\Omega$ goes to zero. By integrating over the thickness of the shield from $x = 0$ to $x = D$ and over acceptable forward scattering angles, from $\Omega = \Omega_i$ to $\Omega = \Omega_f$, where Ω_f is the largest accepted scattering angle, the ratio of events which are scattered through a small angle to the incident flux can be calculated as shown in Eq. 11.

$$\frac{C}{I_0} = \int_{\Omega_i}^{\Omega_f}\int_0^D (e^{-\mu_{t,1}x})(\mu_{t,1}dx)\left(\frac{1}{\sigma_t}\frac{d\sigma_c}{d\Omega}d\Omega\right)(e^{-\mu_{t,2}(D-x)}) \qquad (11)$$

In Eq. 11, C is the rate of events which undergo small-angle Compton scattering in the shield and escape it without further attenuation and I_0 is the incident photon flux. The largest acceptable scattering angle for uranium samples is limited by the 163 keV photpeak. For the proof of principle in this work, $\Omega_f \approx 50^o$ and $\Omega_i \approx 30^o$.

If one assumes that the linear attenuation coefficient does not change after scattering (i.e. $\mu_{t,1} = \mu_{t,2} = \mu_t$), Eq. 11 can be simplified to Eq. 12.

$$\frac{C}{I_0} = e^{-\mu_t D}\int_0^D \mu_t dx \int_{\Omega_i}^{\Omega_f}\frac{1}{\sigma_t}\frac{d\sigma_c}{d\Omega}d\Omega \qquad (12)$$

$$\frac{C}{I_0} = \mu_t D\ e^{-\mu_t D}\int_{\Omega_i}^{\Omega_f}\frac{1}{\sigma_t}\frac{d\sigma_c}{d\Omega}d\Omega \qquad (13)$$
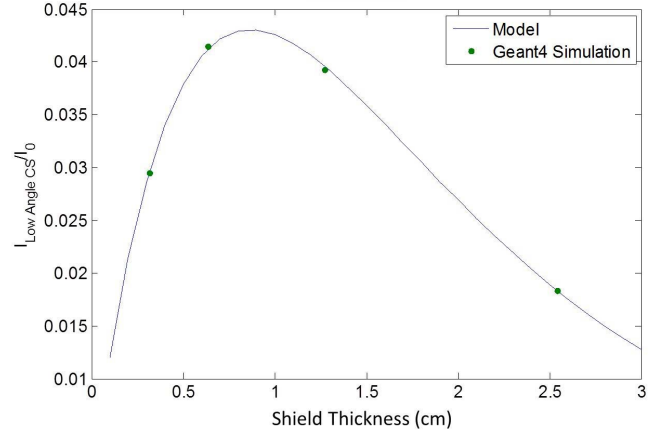

Fig. 6. Proportion of events which undergo small angle Compton scattering in an iron shield versus the thickness of the iron shield. Good agreement between the analytical model and simulation is observed.

Eq. 13 can be thought of as a product of three probabilities. The term $\mu_t D$ is the probability that the photon interacts once within the shield, $e^{-\mu_t D}$ is the probability that the photon traverses the shield without further interactions, and the integral represents the probability that the interaction was a Compton scattering event to within the specified solid angle. These equations were verified using a Geant4 simulation and with measurement data. A demonstration of the agreement between the model and simulated data is shown in Fig. 6.

Rather than compare the rate of events Compton scattered to the incident flux, one must compare it to the unattenuated photon rate exiting the shield because that is what the spectrometer actually measures. The unattenuated photon flux exiting the shield is given by Eq. 14

$$\frac{U}{I_0} = e^{-\mu_t D} \qquad (14)$$

where U is the unattenuated photon flux. Combining Eq. 13 and Eq. 14 results in Eq. 15

$$\frac{C}{U} = \mu_t D\ \frac{1}{\sigma_t}\int_{\Omega_i}^{\Omega_f}\frac{d\sigma_c}{d\Omega}d\Omega = \rho D\ \frac{\mu_t}{\rho}\frac{1}{\sigma_t}\int_{\Omega_i}^{\Omega_f}\frac{d\sigma_c}{d\Omega}d\Omega \qquad (15)$$

where ρ is the mass density of the shield. Eq. 15 can be simplified because the macroscopic mass attenuation coefficient is related to the cross section by Eq. 16

$$\frac{\mu_t}{\rho} = \frac{\sigma_t}{uA} \qquad (16)$$

where A is the relative atomic mass of the shield and u is the atomic mass unit. Finally, because the Klein-Nishina cross section is proportional to the effective atomic number of the shield, the ratio of photons Compton scattered in the forward direction to the unattenuated photon flux is proportional to the mass thickness and atomic number of the shield as shown in Eq. 17.

$$\frac{C}{U} \propto \rho D\ \frac{Z}{uA} \qquad (17)$$

In practice, background-subtracted counts in the 186 keV photopeak and 166-176 keV forward scattered region can be
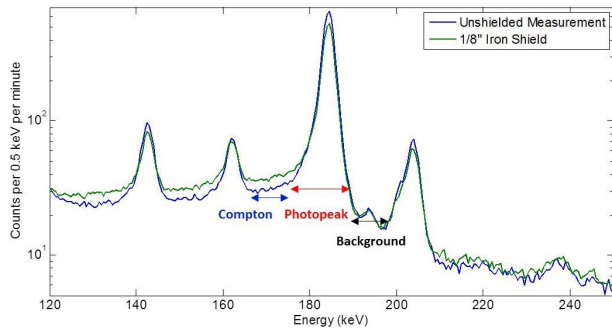
Fig. 7.   Illustration of the regions used to calculate the ratio of source 186 keV source photons that undergo small angle Compton scattering in the intervening material to the unattenuated 186 keV intensity.
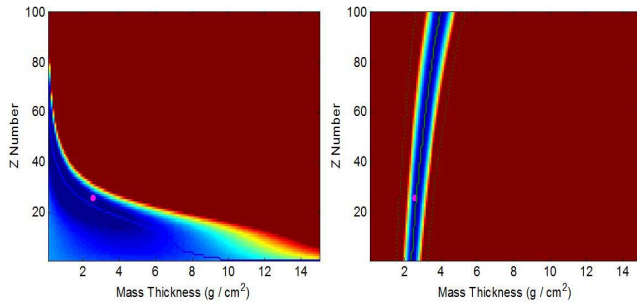

Fig. 8.   Two measurement methods of shielding material and thickness for shields surrounding uranium using peak attenuation ratios (left) and the ratio of Compton scattering to unattenuated photons (right). The correct combination is shown with the magenta dot.
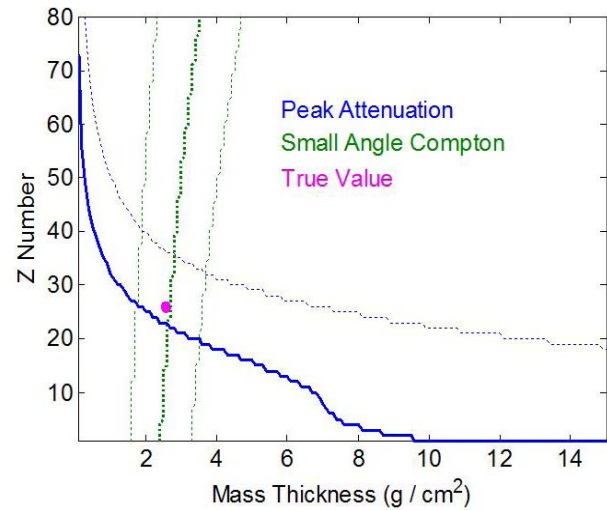

Fig. 9.   Contour plot combining peak attenuation and small angle Compton scattering methods to predict the true composition of shielding material. One sigma uncertainty bars are shown by dotted lines. The magenta dot shows the true mass-thickness and effective atomic number of the shield.
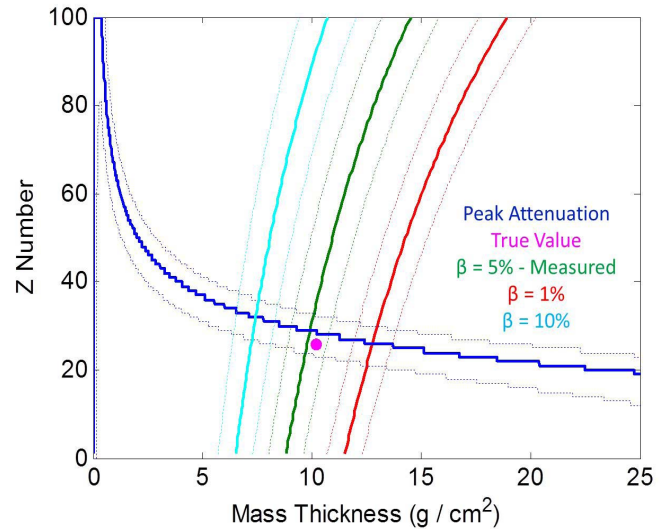

Fig. 10.   Effect of incorrect β factor on shielding identification. In all measurements using the prototype array system, the β factor is about 5% using unshielded experimental results. One sigma uncertainty bars are shown by dotted lines. The magenta dot shows the true mass-thickness and effective atomic number of the shield.

compared. This region of interest was selected because it was below the low energy tail of the 186 keV photopeak and above the influence of the 163 keV photopeak. Also, the 186 keV line is the most prominent, so more source photons will be scattered in the shield from this line than others. In order to account for the photons scattered in the forward direction by the source itself and the detection apparatus, the net counts in the small angle Compton scattering region needs to be multiplied by a factor, β. This β factor was found to be 5% experimentally by measuring the amount of scatter in the 166-176 keV region without a shield present. Eq. 18 describes how to calculate the measured small-angle Compton scattering ratio.

$$\frac{I_{smallangleCS}}{I_{unattenuated}} = \frac{(A_{CS} - B) - \beta(A_{PP} - B)}{(A_{PP} - B)} \quad (18)$$

The left-hand side of Eq.18 is equivalent to the left-hand side of Eq. 17. A_{CS} is the area in the small-angle Compton scattering region, B is the estimated background, and A_{PP} is the area of the photopeak. Fig. 7 demonstrates these regions on a measured uranium spectrum.

One can iterate through Z numbers and mass thicknesses and compare the expected ratio of forward scattered photons to unattenuated source photons with the measured ratio in the same fashion as with photopeak attenuation. The expected ratio is calculated from linear fits of nuclear data based on Eq. 17. A residual plot can be generated as shown in Fig. 8 which provides a range of Z numbers and mass thicknesses

of the shield which can explain the observed spectral effect. Then, one can combine the data from peak attenuation and Compton forward scattering to predict the effective Z number and mass thickness of the shield. The intersection point of the two characteristic lines was calculated and used to estimate the shielding material characteristics as shown in Fig. 9.

Through measurement and simulation, the β factor used to account for self small angle Compton scattering remained relatively unchanged. Simulation predicted the value to be 3%, but measurements indicated 5% was a better estimate. Different source compositions and thicknesses were simulated, and the predicted β factor changed by less than 1%. However, the value used can significantly effect the predicted shielding material. Fig. 10 shows how the β factor can alter the results.
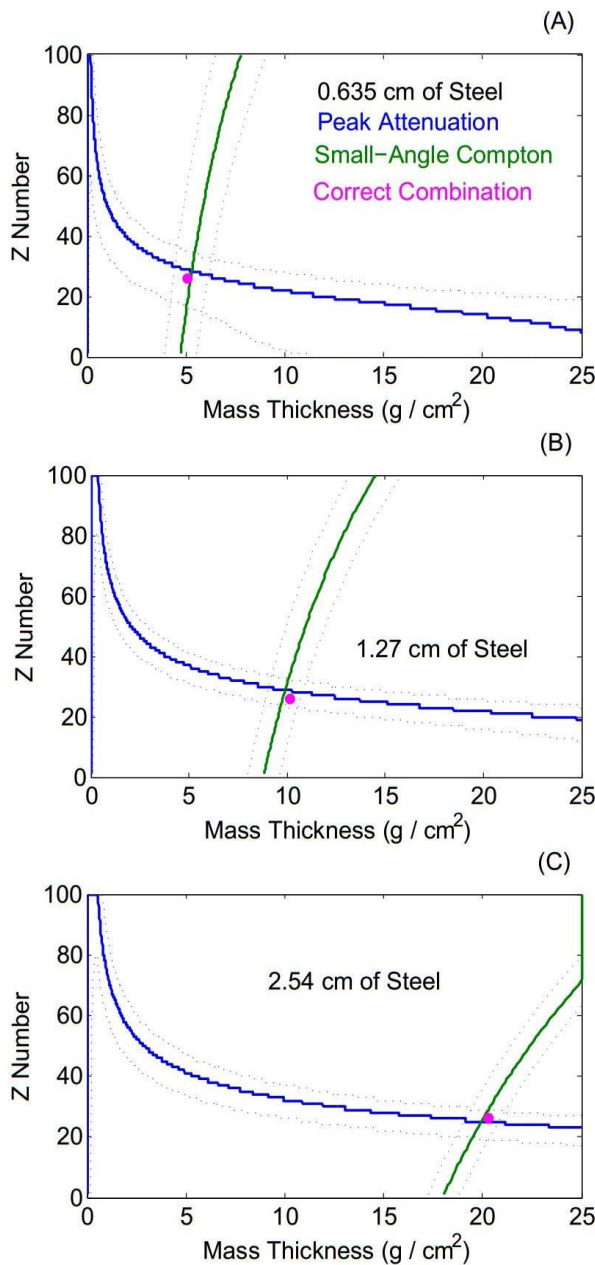
Fig. 11. Contour plot combining peak attenuation and small angle Compton scattering methods to predict the true composition of shielding material for 30×30 cm^2 planar steel shields with thicknesses of 0.635 cm (a) 1.27 cm (b) and 2.54 cm (c). One sigma uncertainty bars are shown by dotted lines. The sample used was a 20 wt% ^{235}U calibration standard at the Y-12 National Security Complex with the shielding material 40 cm from the source and the detector apparatus 50 cm from the source. The magenta dot shows the true mass-thickness and effective atomic number of the shield.

If the β factor is incorrect by 5%, the mass thickness can be incorrect by 4 g/cm^2 while the estimated atomic number of the shield can change by five.

V. URANIUM MEASUREMENTS

This method was demonstrated through real measurements to correctly predict steel thicknesses from an eighth of an inch to one inch. Fig. 11 shows the results of the algorithm for steel shields of various thicknesses. Also, the method was accurate
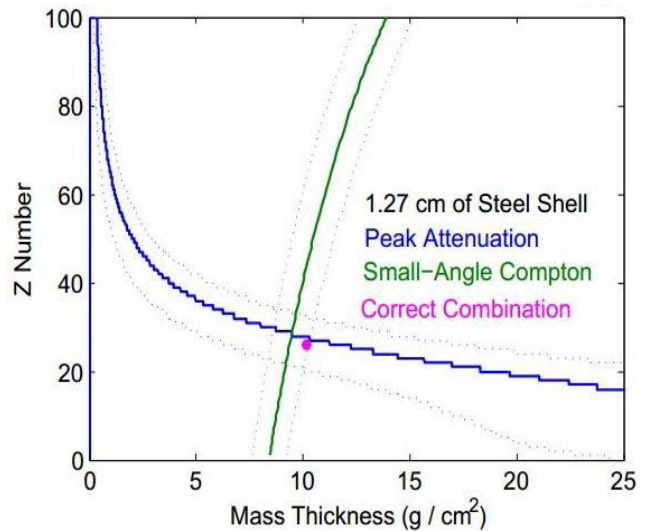

Fig. 12. Shielding characterization algorithm applied to the Rocky Flats HEU shell surrounded with a half inch steel shell. The shell was made of 93 wt% ^{235}U metal with an inner radius of 3 cm and an outer radius of 6 cm. A steel shell, serving as shielding material, encased the Rocky Flats Shell. The detector apparatus was 2 m from the sample. The correct combination for the effective atomic number and mass-thickness of the shield is shown with the magenta dot.

in planar or spherical uranium configurations. The Rocky Flats Shell [18] at the DAF was measured with a 1.27 cm thick steel shell surrounding the highly enriched uranium. The algorithm correctly estimated the mass-thickness and effective atomic number of the shield as shown in Fig. 12.

The method was also applied for aluminum and polyethylene shielded measurements in simulation and experiment and worked adequately for various thicknesses. As shown in Fig. 17, the uncertainty in the effective atomic number is larger for low Z shields. This phenomenon is explored further in Section VI. In simulation, the method did not work as well for lead shields because almost all of the source photons are photoelectrically absorbed rather than Compton scattered. However, in this case, characteristic x-rays could provide some estimate of the intervening material identity and peak attenuations could be used to predict the mass thickness of the shield.

VI. UNCERTAINTY QUANTIFICATION

The uncertainty of the measured shielding parameters can be calculated using the bootstrap method. The recorded gamma-ray spectrum is used as the initial probability density function (PDF) and that distribution is sampled many times. If desired, the other input parameters can be varied as well (the initial expected peak ratios when no shielding is present and the amount of forward scattering caused by the detection apparatus). The method is applied to each sampled spectrum and the shielding parameters are estimated. Then, a histogram can be generated and the uncertainty quantified. Fig. 13 shows the distribution of probable shielding materials from a uranium disk shielded with 1.27 cm of steel shielding. The solid red and green lines show the results of the method using the recorded data. The true shielding parameters are shown
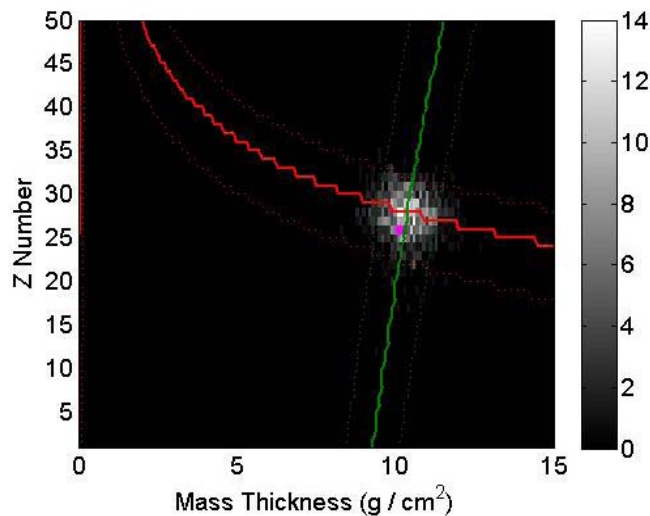
Fig. 13. Histogram of bootstrap sampled spectra results using the described shielding detection method. The solid green and red lines show the results using the recorded data. The binned results are calculated by sampling the PDF created from the recorded data and estimating the shielding parameters from the sampled spectra. The true shielding combination is shown by the magenta dot.

using the magenta dot. One thousand spectra were generated, each with 200,000 events between 0 and 250 keV. Also, this particular estimate allowed the β parameter to vary from a Gaussian distribution with a mean of 5% and a standard deviation of 1% to demonstrate how the uncertainty in the factor propagates to the final answer.

As shown in Fig. 14, there is some bias in the estimate of the mass thickness and effective atomic number of the shielding material. The mass thickness is underestimated for very thick shields because the unattenuated flux is overestimated. The photopeak region is actually comprised of events which are truly unattenuated by the shield, events which are scattered through a very small angle in the shield, and events which are down-scattered from higher energy peaks or from the background. Because the detectors have imperfect energy resolution, some of the events which are forward scattered will be counted as unattenuated counts, even when using the peak area method described in Ref. [14].

To verify this hypothesis, a simulation was conducted in Geant4 for HEU samples shielded by various thicknesses of iron. The simulated spectra were then blurred assuming the resolution of the detector was limited by the 2 keV electronic noise. Then, the net counts in each photopeak were determined. For the simulated spectrum, the net counts can be calculated directly, whereas the peak area method was applied to the blurred spectrum. As shown in Fig. 15, the calculated unattenuated flux for the blurred spectrum is 5% higher than the true unattenuated flux. Since the estimated mass thickness is inversely proportional to the unattenuated flux, an overestimate in the unattenuated flux results in an underestimate in mass thickness. This explains the behavior seen in Fig. 14.

For very thick shields, since most of the signal from the 143 keV and 163 keV gamma-ray lines is attenuated, most of the information for the effective atomic number from the
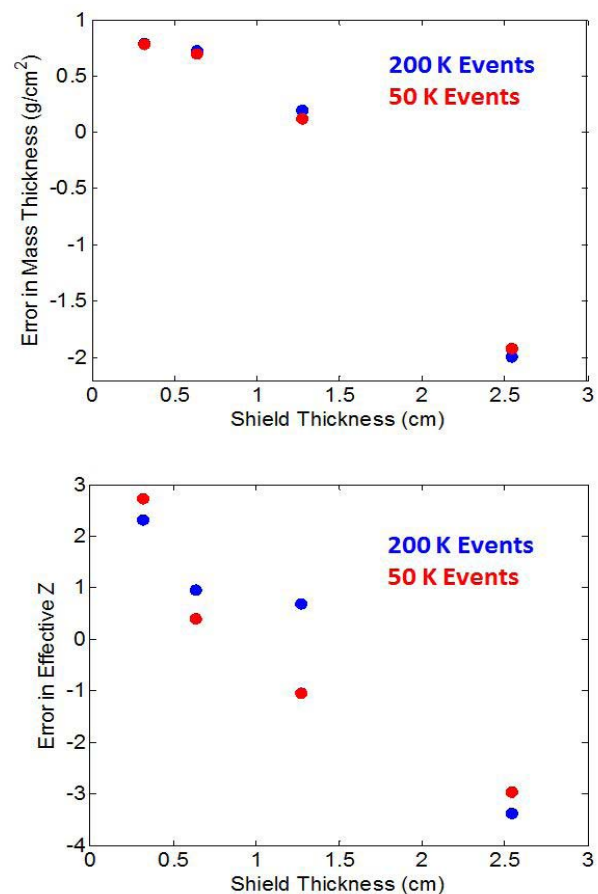

Fig. 14. Systematic errors in the estimate of mass thickness (top) and effective atomic number (bottom) as function of iron shield thickness. The number of events indicated corresponds to the number of events in the spectrum between 0 and 250 keV.
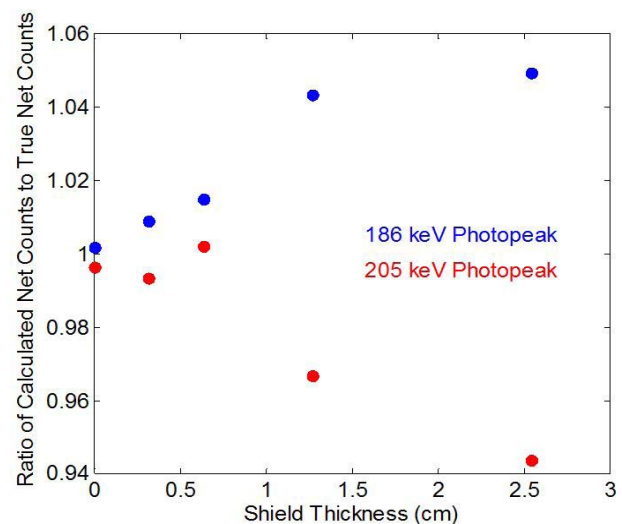

Fig. 15. Ratio of net counts calculated from the blurred spectrum to the true number of unattenuated counts for two uranium gamma-ray lines with various thicknesses of intervening iron shielding.

weighted residuals comes from the 186 keV to 205 keV photopeak ratio. Because the ratio is calculated to be larger than it should be, the effective Z of the shield will also be underestimated. A user can add a correction factor for thick
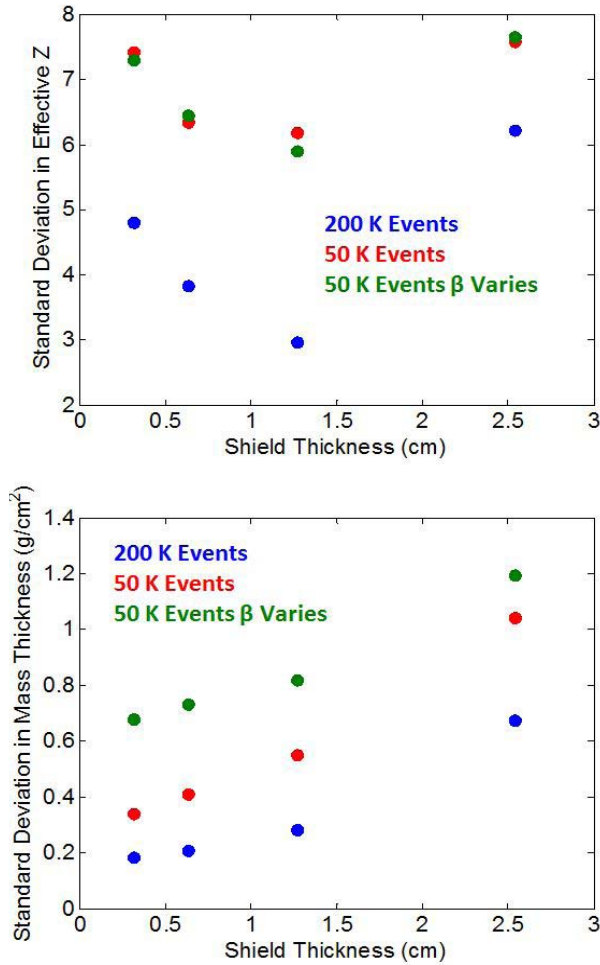
Fig. 16. Standard deviation in calculated effective Z (top) and mass thickness (bottom) as a function of iron shield thickness. In one case, β is allowed to vary about 5% from a Gaussian distribution with $\sigma = 1\%$.
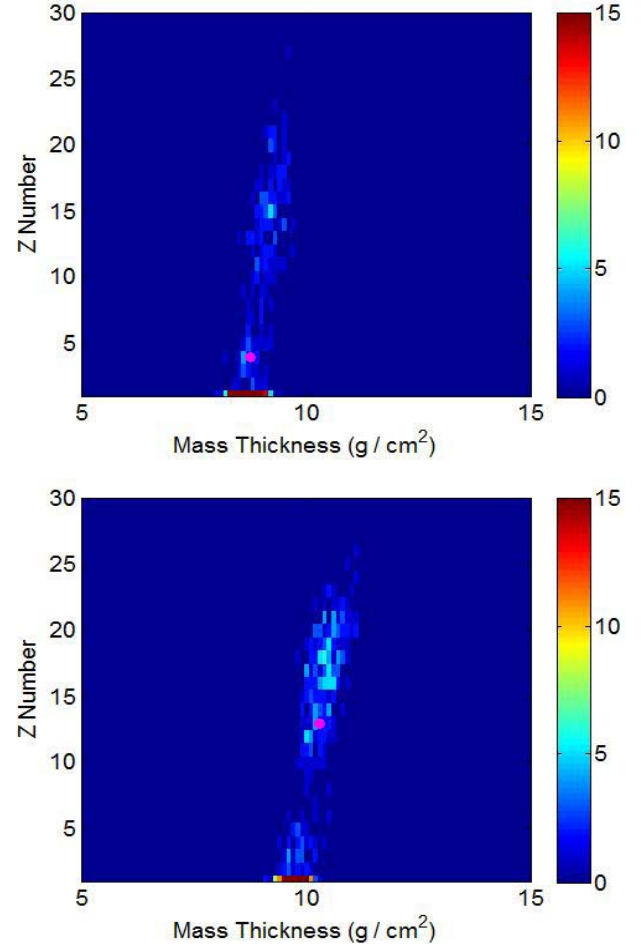

Fig. 17. Histogram of bootstrap sampled spectra results using the described shielding detection method. The binned results are calculated by sampling the PDF created from the recorded data and estimating the shielding parameters from the sampled spectra. The both histograms include 500 trials of spectra with 200,000 events between 0 and 250 keV. A 7.62 cm thick high density polyethylene slab shielded the source in the top histogram whereas the bottom histogram used a 5.08 cm thick aluminum shield. The true shielding combination is shown by the magenta dot. No variation in the β parameter was used for these histograms.

shields to correct for this small effect or use a spectrometer with better energy resolution.

The standard deviation of the calculated shielding parameters as a function of iron shield thickness is shown in Fig. 16. The standard deviation of mass thickness increases for thicker shields because uncertainty in the ratio between Compton scattered events and unattenuated counts increases. The standard deviation of the effective Z has a minimum value. Shields made of this thickness will attenuate enough photons to observe discernible differences in the intensity of the gamma-ray lines, but not so much that the uncertainty in the net counts in the peak is large. The variance in the calculated mass thickness and effective Z is reduced with more events in the spectrum. Also, the variance in the mass thickness is very sensitive to the uncertainty in the β parameter used to account for forward scattering in the detection apparatus when no shield is present.

As shown in Fig. 17, the variance in the calculated effective Z number is quite high for low-Z shields. This is because the attenuation properties do not vary significantly as a function of atomic number for low-Z materials. Therefore, small perturbations in the input spectrum can cause large differences in the calculated Z. However, the estimate of mass thickness

is quite accurate for both cases. The standard deviation for the 3 inch thick polyethylene sheet was only 0.30 g/cm^2 and the standard deviation for the 1.5 inch thick aluminum sheet was 0.41 g/cm^2. The half inch steel sheet, about the same mass thickness as 1.5 inches of aluminum, has a standard deviation of 0.28 g/cm^2. The uncertainty remains unchanged because Compton scattering depends more on the mass thickness than the effective atomic number as shown in Eq. 17.

VII. APPLICATION TO PLUTONIUM MEASUREMENTS

Most plutonium gamma rays are emitted above 300 keV, complicating the use of this algorithm for three reasons. First, the gamma rays will be weakly attenuated by thin shields resulting in more measurement uncertainty. Second, there are more energy bins available for a scattered photon, reducing the probability term in Eq. 9. This will reduce the signal to noise ratio of the small-angle Compton scattering portion of the algorithm. Finally, the harder gamma rays lead to more
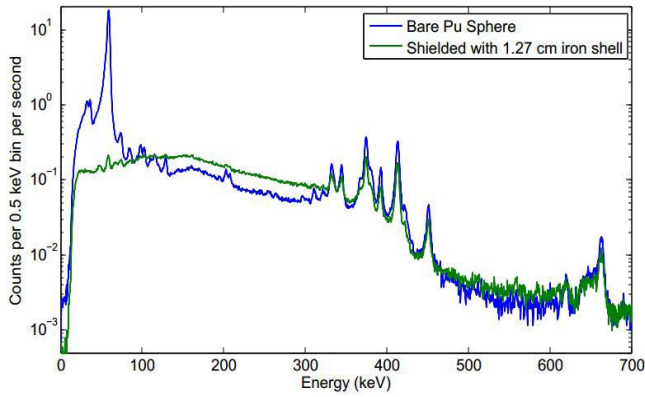
Fig. 18. Measured gamma-ray energy spectrum from a plutonium sample measured with the digital prototype system. The plutonium sample was measured bare and shielded with an 1.27 cm thick iron shell.
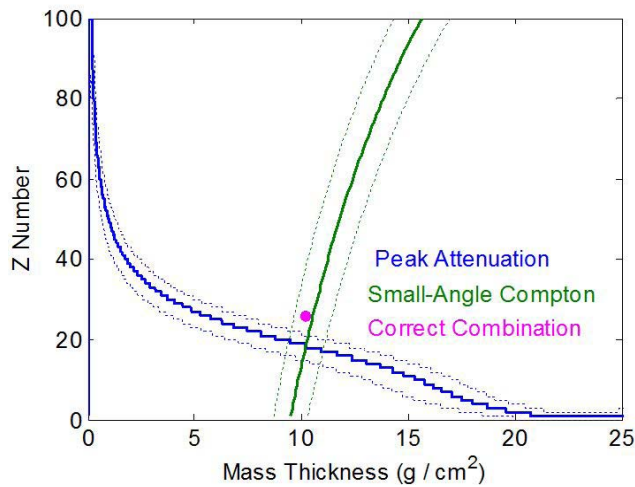

Fig. 19. Contour plot of line attenuation and small-angle Compton scattering algorithms for an iron shell shielding a spherical plutonium sample measured at the DAF. This measurement does not include the 60 keV gamma-ray line from ^{241}Am. The correct combination of effective Z and areal density is shown with the magenta dot.

uncertainty in the initial peak ratios as they will vary more with source thickness.

The 60 keV gamma ray from the decay of ^{241}Am is often the strongest emission from aged plutonium sources [13]. However, if this line is used to determine the shielding materials, one must make another estimate of the plutonium age in order to obtain accurate peak ratios. It is useful to help identify low-Z shields, however.

At the DAF, spherical plutonium sources were attenuated with shells of shielding materials. The main spectral regions used for the attenuation analysis were photopeaks at 129 keV, 312 keV, 332 keV, 393 keV, 451 keV, and a triplet of lines around 375 keV, all signatures of ^{239}Pu. The statistics in the other peak regions were deemed too poor to use. The gamma-ray energy spectra of the bare source and the source shielded with iron are provided in Fig. 18. The region used for small-angle Compton scattering was the triplet of lines at 375 keV. About 6% of these photons will forward scatter to between 350 and 360 keV from the Klein-Nishina formula ($\int_{\Omega_i}^{\Omega_f} \frac{d\sigma_c}{d\Omega} d\Omega$ in Eq. 15 is 6%). The β factor used in Eq. 18 was maintained at 5%. As shown in Fig. 19, the algorithm with

TABLE I
SUMMARY OF METHOD RESULTS USING A 20 wt% ^{235}U SAMPLE AT THE Y-12 NATIONAL SECURITY COMPLEX SHIELDED WITH VARIOUS MATERIALS. IN EACH CASE, 200,000 EVENTS ARE USED IN THE REGION BETWEEN 0 AND 250 keV. THE FIRST FOUR SAMPLES PLANAR STEEL SHIELDS. THE NEXT THREE SAMPLES ARE VARIOUS THICKNESSES OF PLANAR ALUMINUM SHIELDING. THE EIGHTH SAMPLE WAS THREE INCHES OF PLANAR POLYETHYLENE. THE NINTH SAMPLE WAS 1.5 INCHES OF PLANAR ALUMINUM SHIELDING PLUS 2 INCHES OF POLYETHYLENE. THE FINAL SAMPLE WAS 0.25 INCHES OF STEEL PLUS ONE INCH OF ALUMINUM

Areal Density ρx (g/cm^2)	Effective Atomic Number (Z)	Estimated Areal Density (g/cm^2)	Estimated Z_{eff}
2.54	26	3.33 ± 0.18	28.0 ± 5.6
5.08	26	5.81 ± 0.21	26.8 ± 4.2
10.16	26	10.37 ± 0.28	26.7 ± 3.0
20.32	26	18.34 ± 0.68	22.6 ± 6.2
3.42	13	3.21 ± 0.18	10.2 ± 6.5
6.84	13	6.99 ± 0.27	8.8 ± 6.5
10.26	13	10.3 ± 0.41	11.3 ± 7.9
8.76	≈ 4	8.79 ± 0.30	6.95 ± 5.9
12.7	≈ 10	12.37 ± 0.45	10.0 ± 7.5
11.9	≈ 17	12.37 ± 0.43	15.2 ± 7.5

bootstrapping predicts the shield is made of a material with Z number of 19 ± 6 and a mass thickness of 10.2±0.30 g/cm^2. The shield had a Z number of 26 and an areal density of 10.16 g/cm^2.

VIII. CONCLUSIONS

Shielding surrounding SNM can make the material more difficult to detect and complicate its classification. The described algorithm allows one to estimate the effective atomic number and mass-thickness of shielding materials in order to determine unattenuated source emission rates. These rates are important to accurately calculate the source enrichment. Additionally, information regarding surrounding materials can inform the appropriate response to the discovery of SNM in the field.

The described method uses the attenuation of various gamma-ray lines in conjunction with an estimate of the Compton scattering to photoelectric absorption ratio in the shield to estimate the effective atomic number and mass-thickness of the shield. This method has been effectively applied to shielded uranium and plutonium sources and was able to estimate the effective Z and mass-thickness for polyethylene, iron, and aluminum shields of various thicknesses. The standard deviation in the estimated mass-thickness was around 1.3 g/cm^2 whereas the atomic number of the shield was within eight of the true value for steel intervening material. The method is easy to implement on existing high-resolution spectrometers and can obtain more information about the source configuration. The overall attenuation properties of multiple shields can be measured using this method. As shown in Table I, using this method on combinations of shielding material results in the

total areal density of the shield and effective atomic number calculated using a quadrature sum [19]. The key assumptions for this method are that the SNM is roughly infinitely thick to the gamma-ray lines used (or the initial ratios of different energy gamma rays are known) and the number of events Compton scattered through a small angle is not strongly dependent on the source geometry.

The estimate accuracy is improved as the number of photopeak counts improves. Further improvement of energy resolution will also improve the accuracy of this method as net photopeak count rates can be more accurately calculated and there is better energy separation between photopeak events and events which undergo a forward Compton scattering. The accuracy can also be improved in some specific measurement scenarios. If the shield is made of a high atomic number materials, characteristic x-rays can be used to identify the shielding material. Or, if the background and geometry are well known, other Compton scattering energy windows could be used to improve the measurement accuracy.

REFERENCES

[1] R. C. Runkle, D. L. Chichester, and S. J. Thompson, "Rattling nucleons: New developments in active interrogation of special nuclear material," *Nucl. Instrum. Methods, Phys. Res. A*, vol. 663, no. 1, pp. 75–95, 2012.

[2] T. N. Dragnev, "Intrinsic self-calibration of non-destructive gamma spectrometric measurements determination of U, Pu and 241 Am isotopic ratios," *J. Radioanal. Chem.*, vol. 36, no. 2, pp. 491–508, 1977. [Online]. Available: http://dx.doi.org/10.1007/BF02517017

[3] R. Harry, J. Aaldijk, and J. Braak, "Gamma-spectrometric determination of isotopic composition without use of standards," Tech. Rep., 1976.

[4] R. Berndt, E. Franke, and P. Mortreau, "235U enrichment or UF6 mass determination on UF6 cylinders with non-destructive analysis methods," *Nucl. Instrum. Methods, Phys. Res. A*, vol. 612, no. 2, pp. 309–319, 2010.

[5] W. Ruhter, T.-F. Wang, and C. Hayden, "Uranium enrichment measurements without calibration using gamma rays above 100 keV," Lawrence Livermore Nat. Lab., Livermore, CA, USA, Tech. Rep. UCRL-JC-142832, 2001.

[6] K. Nelson, "Shielding and activity estimator for template-based nuclide identification methods," U.S. Patent 8 417 467, Apr. 9, 2013.

[7] S. M. Horne, G. G. Thoreson, L. A. Theisen, D. J. Mitchell, L. Harding, and W. A. Amai, "GADRAS-DRF 18.5 user's manual," Tech. Rep. SAND2014-20625, 2014.

[8] D. N. Anderson, W. K. Hensley, D. S. Barnett, D. K. Fagan, J. I. McIntyre, and J. C. Hayes, "A probabilistic derivation of gamma-ray attenuation and application: Bayesian mass estimation with a low count spectrum," *Nucl. Instrum. Methods, Phys. Res. A*, vol. 569, no. 3, pp. 894–899, 2006.

[9] Y. Zhu and Z. He, "Performance of a 2-keV digitizer ASIC for 3-D position-sensitive pixellated semiconductor detectors," in *Proc. IEEE Nucl. Sci. Symp. Med. Imag. Conf. (NSS/MIC)*, Oct. 2012, pp. 4109–4112.

[10] M. Streicher *et al.*, "A portable 2×2 digital 3-D CZT imaging spectrometer system," in *Proc. IEEE Nucl. Sci. Symp. Med. Imag. Conf. (NSS/MIC)*, Nov. 2014, pp. 1–3.

[11] J. Cantrell, "Uranium enrichment standards of the Y-12 nuclear detection and sensor testing center," in *Proc. 52nd Annu. INMM Meeting*, 2012.

[12] K. P. Ziock, M. T. Burks, C. P. Cork, E. L. Hull, and N. W. Madden, "Performance of gamma-ray imager using a 38×38 crossed-strip Ge detector," in *Proc. IEEE Nucl. Sci. Symp. Conf. Rec.*, vol. 2. Oct. 2003, pp. 1430–1434.

[13] D. Reilly, N. Ensslin, H. Smith, and S. Kreiner, "Passive nondestructive assay of nuclear materials," Los Alamos Nat. Lab., Los Alamos, NM, USA, Tech. Rep. NUREG/CR-5550 LA-UR-90-732, 1991.

[14] G. F. Knoll, *Radiation Detection and Measurement*. Hoboken, NJ, USA: Wiley, 2000.

[15] T. R. C. Johnson *et al.*, "Material differentiation by dual energy CT: Initial experience," *Eur. Radiol.*, vol. 17, no. 6, pp. 1510–1517, 2007.

[16] W. Wang, "Techniques and applications of compton imaging for position-sensitive gamma-ray detectors," Ph.D. dissertation, Univ. Michigan, Ann Arbor, MI, USA, 2011.

[17] S. Agostinelli, "Geant4—A simulation toolkit," *Nucl. Instrum. Methods, Phys. Res. A*, vol. 506, no. 3, pp. 250–303, 2003.

[18] R. Rothe, "Extrapolated experimental critical parameters of unreflected and steel-reflected massive enriched uranium metal spherical and hemispherical assemblies," Idaho Nat. Eng. Lab., Tech. Rep. INEEL/EXT-97-01401, 1997.

[19] R. Murty, "Effective atomic numbers of heterogeneous materials," *Nature*, vol. 207, pp. 398–399, Jul. 1965.

[20] H. Yang, F. Zhang, Y. Zhu, and Z. He, "Efficiency measurement on 6.0 cm^3 3-D CdZnTe detectors," in *Proc. IEEE Nucl. Sci. Symp. Med. Imag. Conf. (NSS/MIC)*, Nov. 2010, pp. 3756–3758.